

Global Mode Analysis of Ion-Temperature-Gradient Instabilities Using the Gyro-Fluid Model in Linear Devices

Tomotsugu OHNO, Naohiro KASUYA¹⁾, Makoto SASAKI¹⁾ and Masatoshi YAGI²⁾

Interdisciplinary Graduate School of Engineering Sciences, Kyushu University, 6-1 Kasuga-Koen, Kasuga, Fukuoka 816-8580, Japan

¹⁾*Research Institute for Applied Mechanics, Kyushu University, 6-1 Kasuga-Koen, Kasuga, Fukuoka 816-8580, Japan*

²⁾*National Institutes for Quantum and Radiological Science and Technology, 2-166 Omotedate, Obuchi, Rokkasho-mura, Aomori 039-3212, Japan*

(Received 19 February 2018 / Accepted 21 May 2018)

In order to understand turbulent transport phenomena in magnetized plasmas, an excitation condition of the ion-temperature-gradient (ITG) instability is investigated in linear device PANTA. Numerical analyses using a global gyro-fluid code in linear devices are performed to obtain mode structures and parameter dependences of the ITG instability. Parameter scans of the linear growth rate show the destabilization condition of the ITG modes. The global analysis considers the boundary condition and determines the radial mode structure, which gives the values of the wavenumber in the direction perpendicular to the magnetic field. The local analysis confirms to reproduce the global analysis result by using the wavenumber obtained from the global analysis. The wavenumber is a parameter in the local model, and the global analysis of the radial mode structure is necessary for the selection of this important parameter.

© 2018 The Japan Society of Plasma Science and Nuclear Fusion Research

Keywords: ion-temperature-gradient instability, finite-Larmor-radius effect, gyro-fluid equation, linear device, radial eigenmode structure

DOI: 10.1585/pfr.13.1401081

1. Introduction

It is important to understand turbulent phenomena in magnetically confined plasmas. A level of turbulent transport is determined by competition of several instabilities and formation of turbulent structures [1]. Fundamental mechanisms of structural formation in turbulent plasmas can be studied in simple cylindrical configurations [2]. Structural formations with nonlinear mode coupling of unstable modes in resistive drift wave turbulence have been revealed by experiments [3–6] and simulations [7, 8] using linear devices. One of the candidates to cause anomalous transport in fusion plasmas is the microscopic instability due to the ion temperature gradient (ITG) [9]. Studies of excitation conditions of the ITG instability have been carried out in basic experiments [10]. The ion temperature can be measured using diagnostics as an ion-sensitive probe [11]. On linear device PANTA [12], ion temperature measurements and numerical analyses of the ITG instability have been progressing. The purpose of our research is to predict excitation conditions of the ITG instability in PANTA. The ITG instability is predicted to be excited when the ratio of the ion temperature gradient to the density gradient exceeds the threshold value near the unity. Numerical simulations by using the fluid model [13] in PANTA shows that a mode with $k_{\perp}\rho_s \sim 1$ can become unstable even in low ion temperature plasmas as in linear

devices [14]. Here, k_{\perp} and ρ_s are the wavenumber in the perpendicular direction to the magnetic field and the effective Larmor radius, respectively. Therefore, a detailed analysis including the finite Larmor radius (FLR) effect is required. Analyses using a set of localized gyro-fluid equations have been carried out [15]. The ion Larmor radius is not much smaller than the plasma radius in the linear device, so the global mode structure must be calculated. In this research, a numerical simulation code is developed to solve global eigen-functions of the ITG instability. A gyro-fluid model [16] without magnetic curvature and nonlinear terms is used as same in Ref. [15]. In Ref. [15] a local assumption for ∇_{\perp} operator gives a single value of k_{\perp} , but in this article combination of various k_{\perp} values is introduced by the Bessel expansion to determine global mode structures. Here we report mode structures and parameter dependences of the ITG instability in PANTA by using the global code.

This paper is organized as follows. In the next section, the set of gyro-fluid equations and the numerical scheme to calculate the radial mode structure are described. In Sec. 3, the excitation condition of the ITG instability is evaluated by linear analyses. In Sec. 4, comparison between the local and global analyses is performed by calculating the ion mass dependence. Finally, we summarize our results in Sec. 5.

author's e-mail: ohno@riam.kyushu-u.ac.jp

2. Global Mode Analysis

2.1 Gyro-fluid model

A set of gyro-fluid equations is derived by taking the moments of the electrostatic gyro-kinetic equation in the velocity spaces [16]. The target plasma has a cylindrical configuration with a homogeneous magnetic field parallel to the axial direction, so the magnetic curvature terms can be eliminated. Applying the gyro-kinetic ordering, the linear forms of the equations in the cylinder are given to be

$$\frac{dn}{dt} + \nabla_{//} u_{//} + \left(1 + \eta_{\perp} \frac{\hat{\nabla}_{\perp}^2}{2}\right) \frac{1}{L_n} \frac{\partial \Psi}{\partial y} = 0, \quad (1)$$

$$\frac{du_{//}}{dt} + \nabla_{//} (\tau n + T_{//} + \Psi) = 0, \quad (2)$$

$$\begin{aligned} \frac{1}{\tau} \frac{dT_{//}}{dt} + \nabla_{//} \left(2u_{//} + \frac{q_{//}}{\tau}\right) + \eta_{//} \frac{1}{L_n} \frac{\partial \Psi}{\partial y} \\ = -\frac{2\nu_{ii}}{3\tau} (T_{//} - T_{\perp}), \end{aligned} \quad (3)$$

$$\begin{aligned} \frac{1}{\tau} \frac{dT_{\perp}}{dt} + \nabla_{//} \frac{q_{\perp}}{\tau} + \left[\frac{\hat{\nabla}_{\perp}^2}{2} + \eta_{\perp} \left(1 + \hat{\nabla}^2\right)\right] \frac{1}{L_n} \frac{\partial \Psi}{\partial y} \\ = \frac{\nu_{ii}}{3\tau} (T_{//} - T_{\perp}), \end{aligned} \quad (4)$$

where n is the ion density, $u_{//}$ is the ion velocity, T is the ion temperature, $\tau = T_{i0}/T_{e0}$, T_{i0} and T_{e0} are ion and electron temperatures at the plasma center, $\eta = L_n/L_T$, L_n is the density gradient length, L_T is the ion temperature gradient length, q is the heat flux, and ν_{ii} is the collision frequency between the ions. The subscripts $//$ and \perp represent the quantities in the parallel and perpendicular direction to the magnetic field, respectively. The time and spatial length are normalized with Ω_{ci} and ρ_s , where Ω_{ci} is the ion cyclotron frequency. Ψ is the gyro-averaged potential $\Psi \equiv \Gamma_0^{1/2} \Phi$, where $\Gamma_0^{1/2} = (1 + b\tau/2)^{-1}$ and $b = -\nabla_{\perp}^2$. Operator b gives the square of the perpendicular wavenumber k_{\perp}^2 , which corresponds to the magnitude of the FLR effect. Two modified Laplacian operators $\hat{\nabla}_{\perp}^2$ and $\hat{\nabla}^2$ are introduced to be

$$\frac{\hat{\nabla}_{\perp}^2}{2} \Psi \equiv -\frac{b\tau/2}{(1 + b\tau/2)} \Psi = \Psi_1, \quad (5)$$

$$\hat{\nabla}^2 \Psi \equiv 2\Psi_1 + \frac{b^2\tau^2/2}{(1 + b\tau/2)^2} \Psi, \quad (6)$$

which are given by the moments of the gyro-averaged $E \times B$ velocity term. The FLR effects are included in Ψ , $\hat{\nabla}_{\perp}^2$ and $\hat{\nabla}^2$ terms. The quasi-neutrality relation is given to be

$$\Gamma_0 \left(n - \frac{b/2}{1 + b\tau/2} T_{\perp} \right) - (1 - \Gamma_0) \frac{\Psi}{\tau} = \Psi, \quad (7)$$

to determine the relation between the density and potential. Collisions are dominant in this system, and higher order moments of the gyro-kinetic equation give simplified forms of the heat flux as follows:

$$q_{//} = -\frac{3}{\nu_{ii}\tau} \nabla_{//} T_{//}, \quad (8)$$

$$q_{\perp} = -\frac{1}{\nu_{ii}\tau} \nabla_{//} T_{\perp}. \quad (9)$$

The following normalizations are used:

$$\begin{aligned} (r, t, n, u_{//}, T_{//}, T_{\perp}, q_{//}, q_{\perp}, \Psi) \\ = \left(\frac{r}{\rho_s}, t\Omega_{ci}, \frac{n_1}{n_0}, \frac{u_{//1}}{c_s}, \frac{T_{//1}}{T_{e0}}, \frac{T_{\perp1}}{T_{e0}}, \right. \\ \left. \frac{q_{//1}}{n_0 T_{//0} c_s}, \frac{q_{\perp1}}{n_0 T_{\perp0} c_s}, \frac{e\Psi}{T_{e0}} \right), \end{aligned} \quad (10)$$

where $c_s = \Omega_{ci}\rho_s$ is the ion sound velocity, and the subscripts 0 and 1 denote the equilibrium and fluctuating component, respectively.

2.2 Numerical scheme

To obtain the linear eigen-mode and -frequency, a spectral code is developed. The Bessel expansion in the r direction and Fourier expansions in the θ, z directions are applied on Eqs. (1) - (4) and (7) by using

$$\begin{aligned} \Phi(r, \theta, z) = \sum_{m=-M}^M \sum_{j=1}^J \sum_{l=1}^L \Phi_{mjl} J_m(\lambda_{mj}r/a) e^{im\theta} \\ \times \cos\left(\frac{\pi}{2}(2l-1)z/L_z\right), \end{aligned} \quad (11)$$

$$\begin{aligned} u_{//}(r, \theta, z) = \sum_{m=-M}^M \sum_{j=1}^J \sum_{l=1}^L u_{//mj} J_m(\lambda_{mj}r/a) e^{im\theta} \\ \times \sin\left(\frac{\pi}{2}(2l-1)z/L_z\right). \end{aligned} \quad (12)$$

Density n and temperature T are also expanded in the same way as in Eq. (11). The equations are solved in the region between $r = 0$ (center of the plasma) and $r = a$ (outer boundary of the plasma). The boundary condition in the radial direction are set to $f = 0$ at $r = 0, a$ when $m \neq 0$, and $\partial f/\partial r = 0$ at $r = 0, f = 0$ at $r = a$ when $m = 0$. Functions $J_m(\lambda_{mj}r/a)$ are used for the expansion to satisfy the boundary conditions, where $J_m(r)$ is the Bessel function, λ_{mj} is the j -th point with $J_m(\lambda_{mj}) = 0$, and m is the azimuthal mode-number. The boundary condition is important in the case when the typical wave length is comparable to the system size. With the parameters for the linear devices, the radial wave length of the unstable mode is comparable to the plasma radius, and the mode structure is strongly restricted by the plasma radius. This is our target for determination of the global radial mode structure, so we put η to be constant in space for simplicity. Periodic boundary conditions are used in the axial direction, and the effect of the end plate is not considered. We solve the matrix of the equations with the spectral expansion using the eigenvalue method. In the eigenvalue method, the eigenvalues of the matrix are obtained using the mathematic library MKL to give the linear growth rate.

For the linearization, the differential operator d/dt and $\nabla_{//}$ are replaced to $i\omega$ and ik_z , where k_z is the wavenumber in the parallel direction. The real and imaginary part of ω give the frequency and growth rate, respectively. The axial mode number is set to l , which gives $k_z = 2\pi\rho_s/L_z$, where

L_z is the device length. Operator b gives

$$b \left[J_m(\lambda_{mj}r/a) e^{im\theta} \right] = -\nabla_{\perp}^2 \left[J_m(\lambda_{mj}r/a) e^{im\theta} \right] = \left(\frac{\lambda_{mj}}{a} \right)^2 J_m(\lambda_{mj}r/a) e^{im\theta}, \quad (13)$$

for the component with azimuthal and radial mode numbers (m, j) , so $\hat{\lambda}_{mj} = \lambda_{mj}/a$ corresponds to the magnitude of k_{\perp} in this model. In the local analysis in Ref. [15], the radial and azimuthal wavenumbers are assumed to be same to reduce a parameter, so k_{\perp}^2 is give as $k_{\perp}^2 = 2k_{\theta}^2 = 2(m/(a/2))^2$.

2.3 Target plasma

The geometry of the plasma is a simple cylindrical shape, and the magnetic field has only the axial component with a uniform intensity. For the simulations, experimental parameters in PANTA are used; device length $L_z = 4.0$ m, plasma radius $a = 0.07$ m, density $n_0 = 1.0 \times 10^{19} \text{ m}^{-3}$, $L_n = 0.07$ m, $v_{ii} = 350 \text{ s}^{-1}$, magnetic field $B = 0.1$ T, temperatures $T_{e0} = 3$ eV and $T_{i0} = 0.3$ eV. The temperatures and magnetic field give $\rho_s = 1.1$ cm, $\rho_i = 3.5$ mm and $\Omega_{ci}/2\pi = 3.8 \times 10^4$ Hz for argon plasmas. With these parameters, $\rho_i/L_n = 0.05 \ll 1.0$, $k_z\rho_i = 5.5 \times 10^{-3} \ll 1.0$ with $l = 1$ and $k_{\perp}\rho_i = 0.02 \ll 1.0$ with $m = 1$, so the gyro-kinetic ordering is satisfied. The other parameters for the analysis are τ and η_i .

3. Linear Instability

Numerical analyses are carried out using the developed gyro-fluid code. Figure 1 shows the dependences of the growth rate on the azimuthal and axial mode number. Here simplification with $\eta_{||} = \eta_{\perp} (= \eta)$ is applied. The mode numbers of the most unstable modes in this parameter are $m = 2$ and $l = 1$. The critical value η_c of the instability in this condition is about 1.2, and the value of the growth rate increases as η increases. The global code can give the radial distribution of T_{\perp} , $T_{||}$, n , $u_{||}$, Φ , and Ψ in addition to the growth rate and eigen-frequency. Figure 2 shows the radial profiles of T_{\perp} , $T_{||}$, n and $u_{||}$ with $m = 2$, $l = 1$, $\eta = 1.2$ and $\tau = 1$ of an argon plasma. The growth rate and frequency are given to be $\omega_i = 2.9 \times 10^{-3}$ and $\omega_r = -9.6 \times 10^{-3}$. Similar results were obtained by the analysis with the local model introducing the k_r value as a parameter.

The ion temperature is the most important parameter for the ITG instability, so the dependency on the magnitude and gradient length of the ion temperature is evaluated. Figure 3 (a) shows the contour plot of the growth rate in the τ and η space. The critical value η_c for the ITG instability changes depending on the magnitude of τ . The minimum of η_c is $\eta_c = 0.8$, and increases as τ increases ($\eta_c = 1.7$, when $\tau = 2.0$, for example). These are the same tendencies as in the local model analyses as in Fig. 3 (b). The cross in Fig. 3 indicates one of the experimental conditions in PANTA ($\tau = 0.1$, $\eta = 0.2$ with an argon plasma).

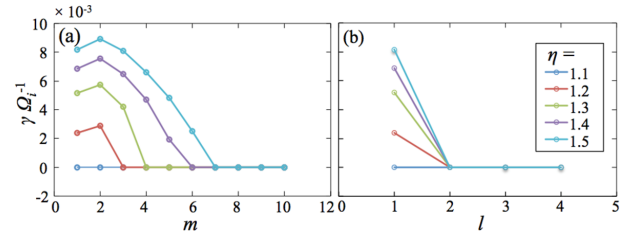


Fig. 1 Dependency of growth rate on m and l with $\tau = 1$, an argon plasma.

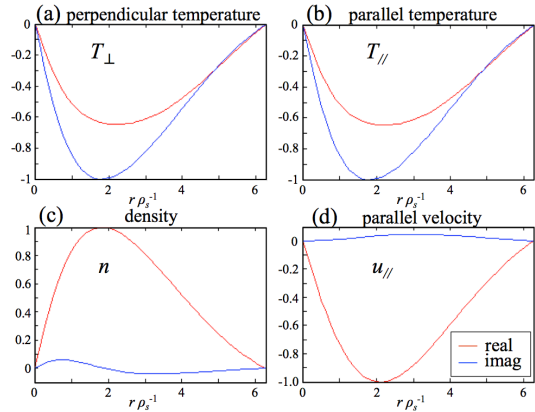


Fig. 2 Radial profiles of eigenmodes of (a) T_{\perp} , (b) $T_{||}$, (c) n and (d) $u_{||}$ with $m = 2$, $l = 1$, $\eta = 1.2$, $\tau = 1$, an argon plasma.

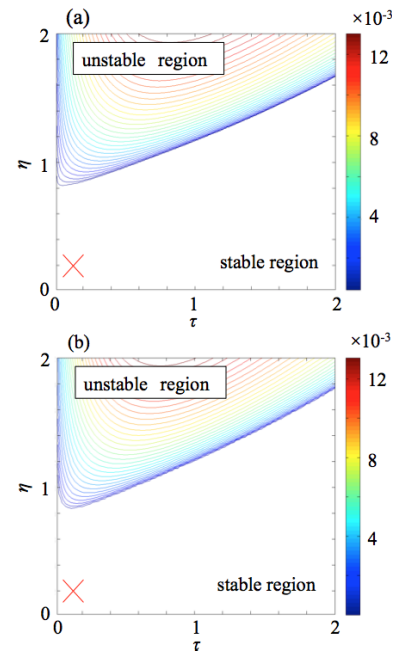


Fig. 3 Contour plot of the growth rate in the τ and η space with $m = 2$, $l = 1$, an argon plasma. The cases with the (a) global and (b) local analysis are plotted.

It suggests that a higher temperature gradient is needed to observe the excitation of the ITG mode in PANTA.

4. Parameter Dependency of Radial Structures

Dependencies on the other experimental parameters are also evaluated. The ion mass depends on the using discharge gas, which makes the Larmor radius different. The effective plasma radius changes, because the spatial length is normalized by the Larmor radius. Figure 4 shows the ion mass dependences of critical η_c with $m = 1 - 5$ in the cases with the global and local analyses. The cases of helium, neon, and argon discharges are plotted. The difference in the dependency on the mode number is partly due to the selection of k_r . In the global model, k_r of the most unstable mode is determined by calculating the eigenmode, though it is only a parameter in the local model. In the case with helium, as shown in Fig. 4, the m dependence is greatly different. The local analysis gives critical value $\eta_c = 1.9$, which is larger than that $\eta_c = 1.2$ in the case with the global analysis, when $m = 1$. This is because the value of k_\perp of the most unstable mode is larger than the value obtained from the relation $k_r = k_\theta$ assumed in the local analysis. Figure 5 shows the relative amplitudes of the k_\perp components in the eigenmodes of the density. The maximum value is normalized to be the unity. $\hat{\lambda}_{mj}$ represents the normalized wave length of the base Bessel functions. As is seen in Fig. 5, there is a peak at $\hat{\lambda}_{mj} = 0.7$, but in the local analysis the smaller value $k_\perp = \sqrt{2}(2m/a)\rho_s = 0.14$ is used. The deviation of k_\perp^2 arises in the higher m modes, because the radial wave length of the unstable mode is also comparable to the plasma size. Figure 5 also shows that the value of $\hat{\lambda}_{mj}$ giving the maximum amplitude is almost the same in spite of the ion mass variation.

In addition, the difference in the treatment of k_θ is the other cause. In the global model, since the radial dependence ($1/r$) in the k_θ terms must be expanded with combination of the various Bessel components, the following relation is used for the azimuthal derivative;

$$\begin{aligned} \frac{\partial}{\partial y} A_j &= \langle ik_\theta A \rangle_j \\ &= i \sum_{k=1}^K \frac{2mA_k}{J_{m+1}^2(\lambda_{mj})} \int_0^1 dr_* J_m(\lambda_{mk}r_*) J_m(\lambda_{mj}r_*). \end{aligned} \quad (14)$$

This calculation gives connection between various Bessel functions. On the other hand, the value of k_θ is given as (m/r) , and is evaluated with a single r value, typically at $r = a/2$ in the local model. The results of the global analysis imply that the difference of the radial structure also affects evaluation of the effective k_θ value. Figure 6 shows the radial profiles of the amplitudes of n when $m = 2$, $l = 1$, $\eta = 1.2$ and $\tau = 1$. In the case of helium, the structure is localized near the center of the plasma in comparison with the cases of argon and neon. This is because the characteristic spatial scale ρ_s is changed. From this result, it is not appropriate under this condition to set the evaluation position of the k_θ value at $r = a/2$ in the local analysis.

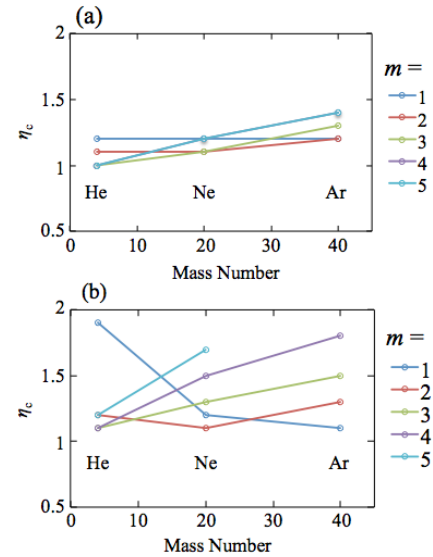


Fig. 4 Ion mass dependences of the critical value η_c , when $\tau = 1$. Those of modes with $m = 1 - 5$ are shown in the case with the (a) global and (b) local analyses.

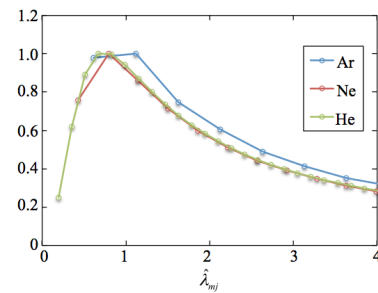


Fig. 5 Relative amplitudes of the k_\perp components in the eigenmodes of the density n , when $\tau = 1$, $\eta = 1.2$, $m = 1$ and $l = 1$. Dependences on $\hat{\lambda}_{mj}$, normalized wave length, are plotted.

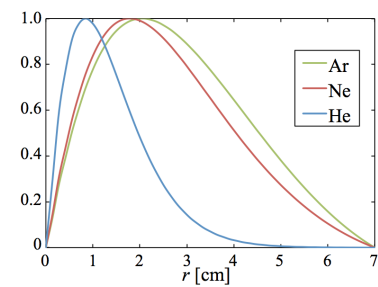


Fig. 6 Radial profiles of amplitudes of the density n with $m = 2$, $l = 1$, $\eta = 1.2$, $\tau = 1$.

Since the differences in the mode structures greatly affect the growth rates of the ITG instability in this way, it can be said that it is meaningful to analyze the detailed mode structures by the global analysis.

5. Summary and Discussion

To investigate the excitation conditions of ITG modes in PANTA linear device, the linear instability analyses were carried out. A gyro-fluid code, which solves global eigen-functions including the FLR effect, was developed and used for the analysis. The same tendency from the local model was obtained, which gives the threshold for the instability in the linear device. Wavenumber k_{\perp} of the most unstable mode was obtained with the radial mode structure analysis. The radial structure is affected by the relative size between the plasma radius (to give the boundary condition) and the Larmor radius (to give the typical spatial length of the instability). The mode is more localized near the center of the plasmas in the case of a discharge gas with a smaller mass number as helium.

The strong restriction by the boundary condition is the main target in this article, and the effect of the background profile is not considered. If the radial dependencies of the density and temperature are introduced, they normally include various Bessel components, so the coupling terms between different Bessel j components in Eqs. (11) - (12) become more complex. The effect of the η profile is important for quantitative evaluation to compare with experiments, and is left for the future work.

From the gyro-fluid model, it was found that the experimental parameters of PANTA are present in the stable region, and for excitation of the ITG instability the η value larger than 4 times is required. In linear machine CLM, the ITG instability has been observed in the case when the radial positions of the steep temperature and density gradient are different from each other to satisfy the excitation con-

dition on η [10]. The condition of destabilization should be explored by the distribution controls of the temperature and density in the future.

Acknowledgments

This work is supported by JSPS KAKENHI Grant Number JP16K06938, and the collaboration program of NIFS (NIFS17KNST112, NIFS16KNXN323) and RIAM of Kyushu University.

- [1] P.H. Diamond *et al.*, Plasma Phys. Control. Fusion **47**, R35 (2005).
- [2] G.R. Tynan, A. Fujisawa and G. McKee, Plasma Phys. Control. Fusion **51**, 113001 (2009).
- [3] T. Windisch, O. Grulke and T. Klinger, Phys. Plasmas **13**, 122303 (2006).
- [4] T. Yamada *et al.*, Nature Phys. **4**, 721 (2008).
- [5] P. Manz, M. Xu, S.C. Thakur and G.R. Tynan, Plasma Phys. Control. Fusion **53**, 095001 (2011).
- [6] Y. Nagashima *et al.*, Rev. Sci. Instrum. **82**, 033503 (2011).
- [7] N. Kasuya *et al.*, Phys. Plasmas **15**, 052302 (2008).
- [8] P. Vaezi, C. Holland, S.C. Thakur and G.R. Tynan, Phys. Plasmas **24**, 092310 (2017).
- [9] W. Horton, Rev. Mod. Phys. **71**, 735 (1999).
- [10] A.K. Sen *et al.*, Phys. Rev. Lett. **66**, 429 (1991).
- [11] N. Ezumi *et al.*, J. Nucl. Mater. **337**, 1106 (2005).
- [12] S. Inagaki *et al.*, Sci. Repts. **6**, 22189 (2016).
- [13] S. Hamaguchi and W. Horton, Phys. Fluids B **2**, 1833 (1990).
- [14] Y. Miwa *et al.*, Plasma Fusion Res. **8**, 2403133 (2013).
- [15] G. Hattori *et al.*, Plasma Fusion Res. **10**, 3401060 (2015).
- [16] W. Dorland and W. Hammett, Phys. Fluids B **5**, 812 (1993).